# Dynamic Tooth Loads and Stressing for High Contact Ratio Spur Gears*‡

R. W. Cornell† and W. W. Westervelt†

One way of possibly improving the structural efficiency, reliability, and power-to-weight ratio of power gear transmissions is to increase their contact ratio. Current spur gearing is usually designed to operate at contact ratios between 1. 2 and 1.6. Contact ratio is defined as the average number of tooth pairs in contact under static conditions and without errors and tooth profile modifications. Thus, a typical contact ratio of 1.5 means that, ideally, two tooth pairs are in contact half of the time, and only one tooth pair is in contact the other half of the time. High-contact-ratio gearing (HCRG) applies to gear meshes that have at least two tooth pairs in contact at all times, that is, contact ratios of 2.0 or more. Because the transmitted load is always shared by at least two tooth pairs for HCRG, the individual tooth loading tends to be less than for present low-contact-ratio gearing (LCRG), thereby potentially decreasing the tooth root and contact stresses. However, HCRG requires gear teeth with lower pressure angles, finer pitch, and increased addendums, all of which increase the tooth stressing per applied load. In addition, HCRG would be expected to be dynamically more sensitive to tooth errors and profile modifications because of the multiple tooth contact.

To properly evaluate HCRG requires two basic analyses: First, a system dynamic analysis is needed to determine the operating load sharing among the two and three tooth pairs in contact, taking into account gear errors and tooth-profile modifications. Second, a stress sensitivity analysis for the gear teeth is needed to convert the dynamic tooth loads to tooth root stresses, taking into account the nonstandard tooth form of HCRG teeth. Such analyses and associated computer program were developed by Hamilton Standard from 1973 to 1975 in support of a NASA Lewis HCRG evaluation study being conducted by Sikorsky Aircraft, Division of United Technologies Corp. (ref. 1). This work was an extension and improvement of the theoretical and experimental work done jointly by M.I.T. (refs. 2 to 4) and Hamilton Standard (refs. 5 and 6) for LCRG from 1959 to 1967. The features of the dynamic system analysis and computer program for HCRG are presented along with some preliminary results from applying the analysis to some typical LCRG and HCRG. These limited results show that the system critical speed, system inertia and damping, and tooth-profile modifications can affect the dynamic gear tooth loads and root stressing significantly.

## Nomenclature

$A,B,C,D$  gear tooth coefficients; see eq. (1)
$a,b,c$  coefficients defined by eq. (10)
$C_d,C_e$  disengagement and engagement cam relief, $\Delta_d/(S_{0d}^2 - S_d^2)$ and $\Delta e/(S_{0e}^2 - S_e^2)$
$d$  viscous damping coefficient of gears, lb·sec/in. (N·sec/m)
$e$  dimensionless tooth error, $e^*/\delta$
$e^*$  tooth error, in. (m)
$i$  number of time history steps in mesh cycle
$J_1,J_2$  polar moment of inertias of gears 1 and 2, in·lb sec2 (kg·m2)
$j$  designate of gear pair in mesh
$k,1/\overline{C}$  single tooth-pair spring rate (reciprocal of compliance), lb/in (N/m)
$k_0,1/\overline{C_0}$  single tooth-pair spring rate at pitch radius (reciprocal of compliance), lb/in (N/m)
$L$  dynamic single tooth load, lb (N)

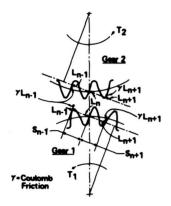| | |
|---|---|
| $L_0$ | static single tooth applied load, $T_1/R_{B1} = T_2/R_{B2}$, lb (N) |
| $M$ | effective linear mass of gear-mesh system, lb sec²/in. (kg/sec² in) |
| $m$ | number of active or engaged tooth pairs |
| $\overline{m}$ | $\displaystyle\sum_{j}^{m} \Phi_j \eta_j$ |
| $N_1, N_2$ | number of teeth on gears 1 and 2 |
| $P_n$ | normal pitch or tooth spacing along line of action ($2\pi R_{B1}/N_1 = 2\pi R_{B2}/N_2$), in. (m) |
| $R_{B1}, R_{B2}$ | base radii of gears 1 and 2 ($R_{p1} \cos \varphi_p$ and $R_{p2} \cos \varphi_p$), in. (m) |
| $R_{p1}, R_{p2}$ | pitch radii of gears 1 and 2, in. (m) |
| $S$ | motion along line of action from pitch line, $R_{B1}\psi_1 = R_{B2}\psi_2$, in. (m) |
| $S_d, S_e$ | distances along line of action from pitch line to the start of disengagement cam and end of engagement cam (positive), in. (m) |
| $S_r$ | linearized relative motion of gears along line of action, $= S_1 - S_2$, in. (m) |
| $S_0$ | reference distance along line of contact for tooth pair compliance coefficients, in. (m) |
| $S_{0d}, S_{0e}$ | distances along line of action from pitch line to end of disengagement cam (tooth tip) and start of engagement cam (positive), in. (m) |
| $T_1/T_2$ | torques on gears 1 and 2, in·lb (N·m) |
| $t$ | time, $S/V$, sec |
| $V$ | tooth velocity along line of action ($R_{B1}\Omega_1 = R_{B2}\Omega_2$), in/sec (m/sec) |
| $w_1, w_2$ | width of gears 1 and 2, in. (m) |
| $x$ | integer cam form exponent |
| $y$ | dimensionless relative motion of gears ($S_r/\delta$) |
| $z$ | deflection of tooth pair versus $S$, in. (m) |
| $\beta_d, \beta_e$ | dimensionless tooth disengagement and engagement cam parameters ($V\sqrt{C_d/\delta/\omega}$)·($V\sqrt{C_e/\delta/\omega}$) |
| $\Delta_d, \Delta_e$ | maximum disengagement and engagement tooth relief for tooth pairs, in. (m) |
| $\delta$ | static deflection of tooth pair under applied load at pitch radius, ($L_0/k_0$), in. (m) |
| $\epsilon_d, \epsilon_e$ | total tooth-profile disengagement and engagement modifications, in. (m) |
| $\eta$ | relative tooth stiffness, $k/k_0$ |
| $\sigma$ | maximum tooth root stress, psi (Pa) |
| $\tau$ | dimensionless time ($\omega t = \omega S/V$) into mesh period, ($\tau_0 + \overline{\tau}$) |
| $\overline{\tau}$ | dimensionless time from $\tau_0$ into mesh period |
| $\tau_c$ | dimensionless mesh time period, $\omega P_n/V$ |
| $\tau_d, \tau_e$ | dimensionless times for start of disengagement cam and end of engagement cam ($S_d\tau_c/P_n$, $S_e\tau_c/P_n$) |
| $\tau_0$ | dimensionless time ($\omega t_0$) into mesh period where $y_0$ and $y_0'$ occur |
| $\tau_{0d}, \tau_{0c}$ | dimensionless times for end of disengagement cam (tooth tip) and start of engagement cam ($S_{0c}\tau_e P_n$, $S_{0e}\tau_c/P_n$) |
| $\lambda$ | $\sqrt{m - \xi^2}$ |
| $\xi$ | viscous critical damping ratio for gears ($d/2\sqrt{k_0 M}$) |
| $\Phi_j$ | function describing tooth-pair contact (1 or 0) |
| $\phi_p$ | pressure angle at pitch radius, rad |
| $\psi_1, \psi_2$ | dynamic angular motion of gears 1 and 2, rad |
| $\overline{\chi}_j$ | function describing tooth cam contact (1 or 0) |
| $\Omega_1, \Omega_2$ | angular rotational speeds of gears 1 and 2, rad/sec |
| $\omega$ | natural angular frequency of mesh system assuming single tooth-pair stiffness ($\sqrt{k_0/M}$), rad/sec |
| $\nabla$ | dimensionless time step ($\tau/i$), where $i = 100$ |

# Theoretical Analysis

The dynamic model for the HCRG system was based on that developed by Richardson and Howland (refs. 2 to 4) but expanded to cover any contact ratios up to four rather than less than two. Similar system dynamic model approaches have been used more recently by other researchers for LCRG (see e. g., refs. 7 and 8). The theoretical model assumes that the two gears act as a rigid inertia and that the teeth act as a variable spring of a dynamic system excited by the nonlinear meshing action and stiffnesses of the gear teeth (see fig. 1).

For simplicity, the real HCRG system of figure 1 was converted into the equivalent rectilinear system of figure 2. The effects of contact ratio, tooth-profile modifications, and tooth errors can be introduced by modifying the size and shape of the cam exterior, which represents the nonlinear meshing action of the teeth.
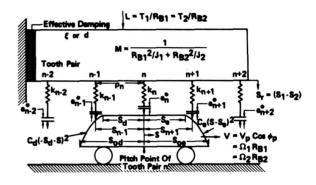


Figure 1. - Free body diagram of mesh for HCRG.          Figure 2. - Dynamic load model for HCRG.

In the earlier analyses of references (refs. 2 and 5) the tooth-pair compliance was assumed constant throughout the mesh; however, because the tooth-pair compliance varies appreciably during the mesh (as shown in figs. 3 and 4), it was decided to include this effect. As these figures show, the variation of tooth-pair compliance with position along the line of action is defined quite adequately by the following five-term power series:

$$\bar{C}/\bar{C}_0 = [1 + A(S/S_0) + B(S/S_0)^2 + C(S/S_0)^3 + D(S/S_0)^4] \tag{1}$$

If the two gears have the same diameter, the tooth-pair compliance is symmetrical about the pitch line, so that $A = C = 0$; otherwise all four coefficients are needed to fit the calculated tooth-pair compliance variation (ref. 9; see fig. 3).

The tooth-profile modification used to ease the tooth loading during engagement and disengagement of the tooth pairs is represented by their respective cams in figure 2. To permit a closed form solution of the differential equation of motion of the gear system, the tooth-profile modifications were represented by cams having the form $C_e(S - S_e)^x$ and $C_d(-S_d - S)^x$, respectively, where $x$ is an integer. Tooth profile modifications represented by noninteger power cams, like 3/2, or complicated forms would be approximated by a series with integer exponents; however, this extra complexity was not required, because typical gear tooth-profile modifications were found to be represented quite well by using simply a cam form with $x = 2$ (fig. 5).

Following the derivation given in reference 2, the differential equation of relative motion between the two gears $S_r = (S_1 - S_2)$ is given by the expression

$$M\ddot{S}_r + d\dot{S}_r + \sum_{j=0}^{m} L_j = L_0 \tag{2}$$

where $L_j$ is the individual tooth loads, $L_0$ is the applied load consistent with the torque on the gears, and $m$ is the number of teeth in contact. For this HCRG study it is assumed that $m$ can have integer
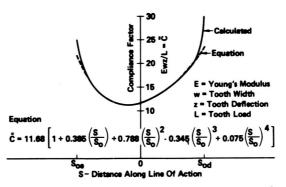
493

Figure 3. - Approximation of compliance of gear tooth pairs for 5.32:1 gear ratio.
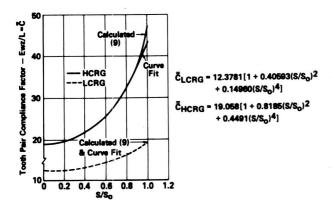


Figure 4. - Approximation of compliance of 8-pitch, 32-tooth LCRG and HCRG tooth pairs for 1:1 gear ratio.
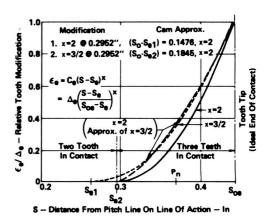


Figure 5. -Approximation of tooth profile modifications for LCRG.

values from 0 to 4. The definition of the parameters and the relationships between the terms of the rectilinear and rotating systems are given in the nomenclature. To simplify the analysis, the sliding tooth friction is assumed negligible, the input and output torques are assumed constant and equal to their average values, and the viscous damping force is assumed proportional to the relative velocity of the two gears, for example, $d(\dot{S}_1 - \dot{S}_2) = d\dot{S}_r$. Equation (2) is put into the following dimensionless form

$$y'' + 2\xi y' + \sum_{j=0}^{m} L_j/L_0 = 1 \tag{3}$$

where $y = S_r/\delta$ and the time parameter, $\tau = \omega t$, is dimensionless so that $y' = dy/d\tau = dy/\omega dt$.

The relative magnitude of the individual tooth loads, $L_j/L_0$, is a function of the tooth stiffness and tooth-profile modification for the particular contact position, $S_j$, the relative gear motion, $S_r$ or $y$, and the tooth errors, $e_j\delta$. The engagement and disengagement tooth-profile modifications, $\epsilon_e$ and $\epsilon_d$, are the same for each tooth pair and are assumed, as discussed above, to be a square function of the distance along the line of action, for example,

$$\epsilon_{je} = C_e(S_j - S_e)^2 \text{ and } \epsilon_{jd} = C_d(S_j - S_d)^2 \tag{4}$$

Thus, the total or combined tooth-pair relief at the start and end of an ideal mesh are

$$\Delta_e = C_e(S_{0e} - S_e)^2 \text{ and } \Delta_d = C_d(S_{0d} - S_d)^2 \tag{5}$$

494

and may be split as desired between the addendum and dedendum tooth modifications of the first and second gears, respectively, or vice versa. The magnitude of the individual tooth load is then given by the expression

$$L_j/L_0 = [y + e_j - \bar{\chi}_j{}^2 \epsilon_{jdcam}/\delta] \eta_j \Phi_j \tag{6}$$

where $\bar{\chi}_j^2$ has a value of 1 or 0, depending on whether the tooth contact is on the profile modification cam or not, and $\Phi_j$, has a value of 1 or 0, depending on whether the tooth pair is in contact or not.

Substituting equation (6) into equation (3) and remembering that $m$ is limited to four teeth, which corresponds to a practical contact limit of four, we find

$$y'' + 2\xi y' = 1 - \sum_{j=n-1}^{n} \Phi_j \eta_j [y + e - \chi^2 \beta_d{}^2]_j - \sum_{j=n+1}^{n+2} \Phi_j \eta_j [y + e - \chi^2 \beta_e{}^2]_j \tag{7}$$

where

$$\chi_{n-1}{}^2 = (\tau - \tau_d + \tau_c)_{n-1}{}^2 = (\omega/V)^2 (S - S_d + P_n)_{n-1}{}^2 \text{ or } 0$$
$$\chi_n{}^2 = (\tau - \tau_d)_n{}^2 = (\omega/V)^2 (S - S_d)_n{}^2 \qquad \text{ or } 0$$
$$\chi_{n+1}{}^2 = (-\tau - \tau_e + \tau_c)_{n+1}{}^2 = (\omega/V)^2 (-S - S_e + P_n)_{n+1}{}^2 \text{ or } 0$$
$$\chi_{n+2}{}^2 = (-\tau - \tau_e + 2\tau_c)_{n+2}{}^2 = (\omega/V)^2 (-S - S_e + 2P_n)_{n+2}{}^2 \text{ or } 0$$

If the $\chi_j$ terms are negative quantities, the teeth are not on the cam or tooth modification, and the corresponding $\chi_j$'s are made equal to zero. If the bracketed term is positive, the tooth pair is in contact and $\Phi_j$ is made equal to 1; otherwise the tooth pair is not in contact and $\Phi_j$ is made equal to zero. Equation (7) is a nonlinear equation because the tooth-pair stiffness ratios $\eta_j$ are a function of $y$.

The above differential equation can be put in the form

$$y'' + 2\xi y' + \sum_j^m \Phi_j \eta_j y = 1 + a + b\tau + c\tau^2 \tag{8}$$

This equation has an instantaneous complimentary solution of

$$y_c = e^{-\xi\tau} (\bar{A} \cos \lambda\tau + \bar{B} \sin \lambda\tau) \tag{9}$$

where $\bar{A} = y_0$ and $\bar{B} = y_0'/\lambda + y_0 \xi/\lambda$, the initial boundary conditions. The instantaneous particular solution of equation (8), which represents the excitation effects, is

$$y_p = \frac{c}{\bar{m}} \tau^2 + \left( \frac{b}{\bar{m}} - \frac{4c\xi}{\bar{m}^2} \right)\tau + \left( \frac{1+a}{\bar{m}} - \frac{2b\xi + 2c}{\bar{m}^2} + \frac{8\xi^2 c}{\bar{m}^3} \right) \tag{10}$$

where $a$, $b$, and $c$ are the following functions of $\eta_j \Phi_j$ and $\bar{\chi}_j^2$:

$$-a = \sum_{j=n-1}^{n} \Phi_j \eta_j [e_j - \bar{\chi}_j{}^2 \beta_d{}^2 q_j{}^2] + \sum_{j=n+1}^{n+2} \Phi_j \eta_j [e_j - \bar{\chi}_j{}^2 \beta_e{}^2 q_j{}^2]$$

495

$$-b/2 = \sum_{j=n-1}^{n} \Phi_j \eta_j \bar{\chi}_j{}^2 \beta_d{}^2 q_j + \sum_{j=n+1}^{n+2} \Phi_j \eta_j \bar{\chi}_j{}^2 \beta_e{}^2 q_j$$

$$c = \sum_{j=n-1}^{n} \Phi_j \eta_j \bar{\chi}_j{}^2 \beta_d{}^2 + \sum_{j=n+1}^{n+2} \Phi_j \eta_j \bar{\chi}_j{}^2 \beta_e{}^2$$

and

$$q_{n-1} = (\tau_d - \tau_c); \quad q_n = \tau_d; \quad q_{n+1} = -(\tau_e - \tau_c); \quad q_{n+2} = -(\tau_e - 2\tau_c)$$

Adding the complementary and particular solutions, the instantaneous dimensionless relative gear motion, $y = y_c + y_p$, is

$$y = e^{-\xi\bar{\tau}} (\bar{\bar{A}} \cos \lambda\bar{\tau} + \bar{\bar{B}} \sin \lambda\bar{\tau}) + \frac{c}{\bar{m}} \tau^2 + \left(\frac{b}{\bar{m}} - \frac{4c\xi}{\bar{m}^2}\right)\tau + \left(\frac{1+a}{\bar{m}} - \frac{2b\xi+2c}{\bar{m}^2} + \frac{8\xi^2 c}{\bar{m}^3}\right) \tag{11}$$

where

$$\bar{\bar{A}} = y_0 - \frac{1+a}{\bar{m}} - \left(\frac{b}{\bar{m}} - \frac{4c\xi}{\bar{m}^2}\right)\!'\!\left(\tau_0 - \frac{2\xi}{\bar{m}}\right) - \frac{c}{\bar{m}}\left(\tau_0{}^2 - \frac{2}{\bar{m}}\right)$$

and

$$\bar{\bar{B}} = \frac{1}{\lambda}\left[y_0' + \xi\bar{\bar{A}} - \left(\frac{b}{\bar{m}} - \frac{4\xi c}{\bar{m}^2}\right) - \frac{2c}{\bar{m}}\tau_0\right]$$

Here, $\tau_0$ is the total dimensionless time into the mesh cycle at which the boundary conditions $y_0$ and $y_0'$ are defined. Also $\bar{\tau}$ is the dimensionless time measured from this instant of time, so that the total dimensionless time into mesh is $\tau = \tau_0 + \bar{\tau}$. If there are no tooth pairs in contact, for example, $\bar{m} = \sum_j^m \Phi_j \eta_j = 0$, the solution of equation (8) is

$$y = y_0 + [\bar{\tau} - (1/2\xi - y_0')(1 - e^{-2\xi\bar{\tau}})]/2\xi \tag{12}$$

Because of the variable tooth-pair stiffnesses during the mesh, differential equation (8) is nonlinear so that the above solutions apply for an instant in time; for example, the solutions continually change during the repetitive mesh period $P_n$ or $\tau_c$. Also, because the number of active tooth pairs and the excitations vary throughout the mesh cycle, the closed form solutions (eqs. (11) and (12)) are piecewise continuous. Thus, to solve this piecewise, nonlinear problem, it was decided to use a time history solution and step through the mesh cycle in small dimensionless time increments of $\nabla = \bar{\tau}_c/i$, where $i$ was made 100. During each time increment the tooth stiffnesses were assumed to be the appropriate constant values given by $\eta_j$. In this way the above closed form solutions given by equations (11) and (12) can be used for determining the relative dynamic gear motion $y$ and velocity $y'$ by replacing $\tau$ by $\nabla$, thereby circumventing the progessive error that can develop by numerically integrating the differential equation (see refs. 2 to 5). To obtain the appropriate values of $\eta_j$, it is necessary to define the position of each tooth pair along the line of action, $S_j/S_0$, and apply equation (1), where $\eta_j = k_j/k_0 = \overline{C_0}/\overline{C_j}$.

To step the above closed form equations for the dynamic gear motion through one mesh of "$i$" increments, one must know the initial conditions $y_0$ and $y_0'$ at $\tau = 0$. These can only be obtained by iteration on the basis that, after the passage of one gear mesh, $P_n$, or gear-mesh time, $\tau_c$, the gear

displacement and velocity must be the same as that for the starting condition, if no gear errors are involved. Thus, the procedure is to assume initial values of $\bar{y}_{01}$ and $\bar{y}'_{01}$, calculate sequentially the gear motion for the $i$ time steps in the mesh, and obtain the values of $\bar{y}_{i1}$ and $\bar{y}'_{i1}$ at the end of the mesh cycle. Usually, a good first approximation for the initial assumed values of $\bar{y}_{01}$ and $\bar{y}'_{01}$ are the reciprocal of the theoretical contact ratio and zero, respectively. In order to assure convergence, the second initial values for the iteration are made the average of the assumed beginning and calculated ending values from the first iteration, that is,

$$\bar{y}_{02} = (\bar{y}_{01} + \bar{y}_{i1})/2 \text{ and } \bar{y}_{02}' = (\bar{y}_{01}' + \bar{y}_{i1}')/2 \tag{13}$$

This process is repeated until the difference between the initial and final values are within a small prescribed amount. An iteration difference of 0.002 for both dimensional quantities has been found to give satisfactory results.

Once the relative gear motion, $y$, has been determined for each of the $i$ time steps through the repetitive mesh, $P_n$, the relative tooth loads, $L_j/L_0$, can be obtained by using the $\Phi_j$ terms given in equation (7), including the appropriate value of $\Phi_j$, that is, 1 or 0. This iterative procedure applies only for cases for no tooth errors; for if there are tooth errors, the motion at the end of a given mesh will not be the same, in general, as that at the beginning of the mesh. The solution for the case with tooth errors is done in two steps: First, the iterative solution is obtained for the zero error case as described above. Then, starting with the known initial conditions of $\bar{y}_0$ and $\bar{y}_0'$ the analysis is run on a consecutive mesh basis, introducing the specified error on any tooth or teeth desired.

The above dynamic load analysis for HCRG with arbitrary contact ratios between 1 and 4 was programmed for the IBM 370–168 using Fortran. The program has three operating modes:

The basic mode option is for HCRG without tooth spacing erros The output in this case is a listing of the convergence process, if desired, for obtaining $\bar{y}_0$ and $\bar{y}_0'$ and the converged results with plots of the results, if requested.

The basic/error mode option first performs the the basic mode option to obtain the converged initial conditions and then runs eight tooth passages using the specified tooth spacing errors. The output consists of that for the basic mode option plus the results for the eight tooth passages with plots, if requested.

The error mode option requires initial converged input gear displacement and velocity from the basic mode option and then proceeds to calculate the dynamic tooth results for eight tooth passages using the specified tooth spacing errors. In order to reduce the printout of 100 time increments per mesh with plots, if desired, all three modes of operation have the option of only listing the maximum for each gear in the mesh. The cpu time to run each constant speed and torque case varies with the operating mode, but usually is less than 1 second.

Because the relationship of tooth root stressing per load varies significantly with load position on the tooth, the maximum tooth root stressing and tooth loading usually occur at different times during the mesh cycle. It appeared desirable, therefore, to include a postprocessor in the computer program to convert the individual tooth loads to tooth root stresses. Since the tooth forms for HCRG deviate appreciably from the conventional tooth forms, it was decided to use an improved and simplied version of the Heywood analysis for tooth stressing (ref. 10) because it includes most of the factors that affect stressing. A subsequent paper will give the details of this modified version of the Heywood gear tooth stress analysis. Figure 6 presents a comparison of the stress per load versus load position for both a HCRG and LCRG using various conventional methods of stress analysis and the modified Heywood analysis. The modified Heywood method gives results that agree well with those based on the Heywood and Kelly methods, which, in turn, have been found to correlate well with test results. The results in figure 6 also show that the relationship between the Heywood analyses and the usual Lewis or AGMA analyses differ significantly for the low- and high-contact-ratio gears, being about 20 to 28 percent higher for the LCRG and about 10 to 18 percent higher for the HCRG, respectively. These differences support the need for an accurate stress sensitivity analysis for general involute spur gear teeth, which the modified Heywood analysis is believed to give.

In the computer program, provisions had to be made for the stress analysis of three different gear tooth configurations (fig. 7). One version assumes no undercutting in the fillet region of the
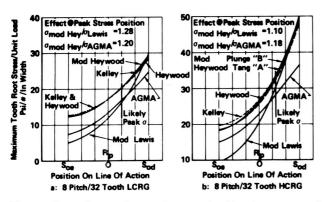
Figure 6. - Comparison of gear tooth stress sensitivities for different analysis methods.
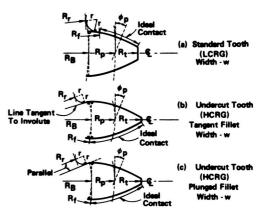


Figure 7. - Gear tooth geometries.

tooth, which is usually the case for conventional LCRG. The two other versions were developed to cover undercut teeth, one in which the undercut is made tangent to the involute tooth profile and the other in which the undercut is made by plunging the fillet cutter parallel to the fillet radius centerline (figs. 7(b) and (c)). The computer program determines whether the tooth requires undercutting and uses the proper tooth geometry in the stress sensitivity calculation. The tangent undercut tooth geometry is used unless the plunged undercut tooth geometry is specified, because it results in slightly lower stressing.

For completeness the postprocessor in the program is being expanded to calculate the variation of $PV$ and contact stress as well as tooth fillet stress with contact position. Presently the computer program only gives the results for one of the gears, so that two runs are required; therefore, the program is also being modified to give results for both the gears at the same time.


## Application of Analysis

The above analysis and computer program was used to investigate the dynamic tooth loads and stressing of a LCRG and initially four HCRG for a speed ratio of one. The LCRG had a gear-mesh contact ratio of 1.566, and the HCRG had a gear-mesh contact ratio of 2.40. All the gears had a 4-in. pitch diameter and a 3/8-in. width. The design torque load, $T$, was 2400 in·lb.

The maximum combined gear tooth-pair profile modification or relief, $\Delta_T$, was based on the statistical sum of the tooth errors, $\Delta_e$, and the maximum static deflection of the teeth, $\Delta_d$, as given by the equation

$$\Delta_T = \Delta_d + \Delta_e = \left[ \frac{fT}{R_p \sum_{j}^{*} k_j} + \sqrt{\sum_{\mu} e_{\mu}^2} \right] \tag{14}$$

In equation (14) $\sum_{j}^{*} k_j$ is the sum of the engaged tooth stiffnesses at a static gear contact position just before the number of teeth in contact increases by one, and the $e_{\mu}$'s are the various kinds of tooth errors. For this study the load factor, $f$, was assumed equal to 3/2. The tooth errors were assumed to be profile, $\pm 0.0001$ in.; spacing, $\pm 0.0003$ in.; and lead, $\pm 0.0001$ in., which results in a statistical total of $\sqrt{\sum_{\mu} e_{\mu}^2} = 0.00033$ in. The gear tooth stiffnesses (ref. 9) versus load position for the 8-pitch, 32-tooth LCRG and the 8-pitch, 32-tooth HCRG are given in figure 4. The pertinent parameters for the LCRG and initial four HCRG's are given in table 1. The length of tooth-profile modification is presented in terms $S_d/S_{0d}$ and $S_e/S_{0e}$, which can vary from 0 to 1 depending on where the profile modification starts, being zero if it starts at the pitch radius and 1 if it starts at the tip or root. The "long" tooth-profile modification for the HCRG simulated the 3/2 power profile modification (fig. 5); the "short" tooth-profile modification corresponded to the standard practice of starting the modification where the theoretical number of teeth in contact changes by one, that is, 1 to 2 or 2 to 3, for the LCRG and HCRG, respectively.

498

Table 1 Characteristics of LCRG and HCRG designs; $R_{p1} = R_{p2} = 2.00''$ and $w = 0.375''$

| Parameter | LCRG | HCRG-1 | | HCRG-2 | |
|---|---|---|---|---|---|
| Tooth Profile Mod. | Standard | Standard-Short | Long - X=3/2 | Standard | Long - X=3/2 |
| Diametral Pitch | 8 | 8 | 8 | 10 | 10 |
| Teeth, N | 32 | 32 | 32 | 40 | 40 |
| Contact Ratio | 1.566 | 2.40 | 2.40 | 2.40 | 2.40 |
| Pressure Angle, $\phi_p$ | 22.5° | 20° | 20° | 20° | 20° |
| Tooth Thickness, $t_p$ | 0.1933" | 0.1933" | 0.1933" | 0.1541" | 0.1541" |
| Normal Pitch, $P_n$ | 0.3628" | 0.3690" | 0.3690" | 0.2952" | 0.2952" |
| Base Radius, $R_B$ | 1.8478" | 1.8794" | 1.8794" | 1.8794" | 1.8794" |
| Tip Radius, $R_t$ | 2.1250" | 2.1914" | 2.1914" | 2.1472" | 2.1472" |
| Fillet Radius, r | 0.0605" | 0.0630" | 0.0630" | 0.0480" | 0.0480" |
| Radius to Fillet, $R_r$ | 1.8417" | 1.7907" | 1.7907" | 1.8342" | 1.8342" |
| Rad. to Fillet Cont. $R_f$ | 1.9094" | 1.8948" | 1.8948" | 1.9056" | 1.9056" |
| Length Mod., $d_a = d_d$ | 0.2054" | 0.14776" | 0.18466" | 0.11818" | 0.14756" |
| Mag. Mod., $\Delta_a = \Delta_d$ | 0.00237" | 0.00216" | 0.00216" | 0.0020" | 0.0020" |
| Cam Coef., $C_a = C_d$ | 0.05628" | 0.09893" | 0.06334" | 0.14339" | 0.09186" |
| Start Cam, $S_a = S_d$ | 0.0787" | 0.29514" | 0.25824" | 0.23620" | 0.20874" |
| End Cam, $S_{pa} = S_{pd}$ | 0.2841" | 0.4429" | 0.4429" | 0.3543" | 0.3543" |



Figure 8. - Effect of applied torque on dynamic gear tooth load for 8-pitch, 32-tooth LCRG. M = 0.001 lb sec$^2$/in.; $\xi$ = 0.10.
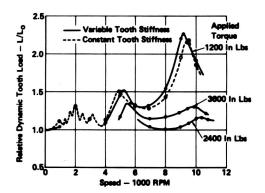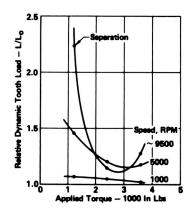


Figure 9. - Effect of speed on dynamic gear tooth load for 8-pitch, 32-tooth LCRG. M = 0.001 lb sec$^2$/in.; $\xi$ = 0.10.
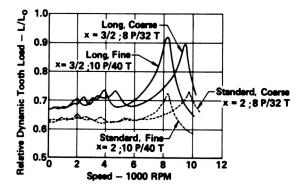


Figure 10. - Effect of speed on dynamic gear tooth load for coarse and fine HCRG. M = 0.001 lb-sec$^2$/in.; $\xi$ = 0.10; T = 2400 in-lb.

The loading and stressing of a gear tooth can vary appreciably with speed, damping, load, and inertia because of the dynamic action. It is impossible, therefore, to compare gear designs unless these operating parameters are varied over their realistic ranges. In general, for a given tooth design the system inertia shifts the system natural frequency and, thus, the subharmonic response peaks of the system, and the amount of damping determines the magnitudes at these response peaks. Also, as the applied load increases, the dynamic load and root stressing per applied load usually decrease until the tooth-profile modification becomes inadequate for the higher loads (figs. 8 to 10). At low loads and sometimes at the system response peaks, complete separation of the gear teeth can occur for low system inertias and damping.

The variation of dynamic tooth loadings with speed for LCRG and HCRG are given in figures 9 and 10 for low system inertias. These figures show that the primary resonance response occurs around 9000 rpm and varies significantly with applied load and tooth modification. Figure 9 also shows the effects of using a constant tooth-pair stiffness based on the pitch radius (refs. 2 to 5) compared with the realistic variable tooth stiffness. Apparent is the slight increase in natural frequency and slightly lower response using the constant stiffness instead of variable stiffness. Also, because of the variable tooth stiffness, the subharmonic critical speeds are not integer reciprocals of the primary critical speed, as they are for a constant tooth stiffness. Apparent in figures 9 and 10 is the significant shift in natural frequency of the system with the magnitude of the applied load and tooth modification due to the nonlinear effects of the variable tooth stiffness. Figure 10 shows that for the HCRG the short (square power) tooth-profile modification results in appreciably lower dynamic tooth loads than the long (3/2 power) tooth-profile modification. This figure also shows
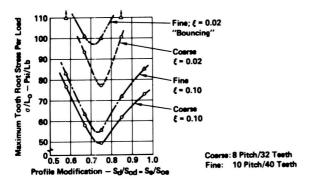
Figure 11. - Effect of profile modification length on dynamic tooth stressing of coarse and fine HCRG. M = 0.001 lb-sec$^2$/in.; N = 9500 rpm; T = 2400 in-lb.
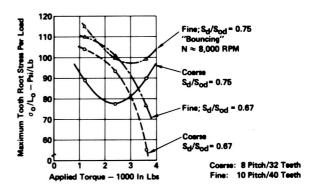


Figure 12. - Effect of applied torque on dynamic tooth stressing of HCRG. M = 0.001 lb-sec$^2$/in.; $\xi$ = 0.02; N = 9500 rpm.

**Table 2  Comparison of tooth root stressing of LCRG and HCRG for primary response at $\sim$ 9500 rpm; $M$ = 0.001 lb s$^2$/in.**

| Maximum Tooth Root Stress | Parameter | Tooth Error | LCRG 8 Pitch/ 32 Teeth | HCRG 8 Pitch/ 32 Teeth | HCRG LCRG |
|---|---|---|---|---|---|
| —— | Contact Ratio, CR | —— | 1.566 | 2.40 | —— |
| —— | Pressure Angle, $\phi_p$ | | 22.5° | 20.0° | —— |
| —— | Profile Mod. Length, $S_d/S_{od}$ | | 0.28 | 0.75 | —— |
| $\sigma_0$ | T = 2400 in lbs; $\xi$= 0.10 | None | 58.8 Ksi | 55.2 Ksi | 0.94 |
| | T = 2400 in lbs; $\xi$= 0.02 | | 98.7 Ksi | 86.8 Ksi | 0.88 |
| | T = 3600 in lbs; $\xi$= 0.02 | | 159.7 Ksi | 152.2 Ksi* | 0.95 |
| $\sigma_e/\sigma_0$ | T = 2400 in lbs; $\xi$= 0.10 | 0.00042" | $\sim$ 1.07 | $\sim$ 1.11 | 1.04 |
| | T = 2400 in lbs; $\xi$= 0.02 | | $\sim$ 1.00 | $\sim$ 1.07 | 1.07 |

* For $S_d/S_{od}$ = 0.67

**High Contact Ratio Gear (2.4)**
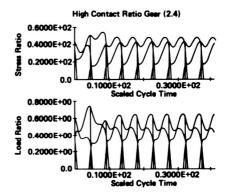


Figure 13. - Effect of tooth errors on dynamic tooth loads and stressing of HCRG.  M = 0.001 lb-sec$^2$/in.; u = 0.02; N = 10 000 rpm.

that the coarser, 8-pitch design is probably stronger than the finer 10 pitch design because the dynamic loads are slightly lower and its teeth have lower stress sensitivity.

Because the length of the tooth-profile modification appeared to affect significantly the dynamic gear loads, its effect was investigated further for both the coarse- and fine-tooth HCRG designs. The evaluation was made at the primary critical speed of about 9500 rpm by analyzing designs with $S_e/S_{0e} = S_d/S_{0d} = 0.58$, 0.67, 0.75, 0.85, and 0.96. The effects of applied load and damping were also included in the study. The effect of the start of the tooth-profile modification on the maximum tooth root stress per applied load is given in figure 11 for low and high dampings of $\xi = 0.02$ and 0.10, respectively, and for the design torque load of 2400 in·lb. These results show that the optimum tooth-profile modification for both HCRG designs occurs at a $S_e/S_{0e} = S_d/S_{0d} = 0.75$ rather than the usual value of 0.67. Thus, the optimum length of tooth-profile modification for HCRG is about 75 percent of that based on the change in the number of teeth in contact. These results show that system damping has a large effect on the tooth root stressing. The results for the fine 10-pitch HCRG with low damping deviates from the other results because of gear separation or bouncing. For a damping of $\xi = 0.10$ figure 11 shows that the tooth root stressing of the course 8-pitch HCRG is 10 percent lower than for the fine 10-pitch HCRG. The effect of applied load on the maximum tooth stressing for the 8- and 10-pitch HCRG at their primary response is given in figure 12 for low damping of $\xi = 0.02$. It is apparent that the length of the profile modification should be increased for higher applied loads, $S_d/S_{0d} = 0.75$ being optimum for 2400 in·lb of torque whereas $S_d/S_{0d} = 0.67$ is optimum for 3600 in·lb of torque. A similar study of the 8-pitch LCRG showed that its length of profile modification was optimum for the design torque of 2400 in·lb, thus substantiating that HCRG should have shorter profile modifications than LCRG.

Comparison of the maximum root stressing of LCRG and HCRG at their primary response peaks are given in table 2 for various applied loads, damping, and tooth errors and assuming the optimum profile modification for each gear design. For no tooth errors, the HCRG tooth root stressing is 6 to 13 percent lower than that for the corresponding LCRG, the degree of improvement depending on the applied load and damping. However, the dynamic analysis shows the HCRG is about 5 percent more sensitive to typical tooth errors than the LCRG. Thus, unless tighter manufacturing tolerances are used to minimize the HCRG tooth errors, its tooth root stressing will be only a few percent less than that for LCRG. Figure 13 shows a typical tooth-load and root-stress history computer plot for a HCRG with tooth error. It shows that the aberrations are damped out in about four mesh cycles, even for a low damping of $\xi = 0.02$. These results illustrate very clearly that the stress and load peak at different times during the mesh cycle and are influenced quite differently by tooth errors.

## Conclusions

An analysis and computer program has been developed for calculating the dynamic gear tooth loading and root stressing for HCRG as well as LCRG. The analysis includes the effects of the variable tooth stiffness during the mesh, tooth-profile modification, and gear errors. The calculation of the tooth root stressing caused by the dynamic gear tooth loads is based on a modified Heywood gear tooth stress analysis, which appears more universally applicable to both LCRG and HCRG. The computer program is presently being expanded to calculate the tooth contact stressing and PV values.

Sample application of the gear program to equivalent LCRG (1.566 contact ratio) and HCRG (2.40 contact ratio) revealed the following:

1. The operating conditions and dynamic characteristics of the gear system can affect the gear tooth loading and root stressing, and therefore, life significantly.

2. The length of the profile modification affects the tooth loading and root stressing significantly, the amount depending on the applied load, speed, and contact ratio.

3. The effect of variable tooth stiffness is small, shifting and increasing the response peaks slightly from those for constant tooth stiffness.

4. The stress sensitivity analysis methods used for gear teeth can influence appreciably the dynamic stress comparison of LCRG and HCRG.

5. The tooth loading and root stressing for HCRG are affected more adversely by gear errors than for LCRG.

6. The errorless, coarse, 8-pitch HCRG has a root tooth stress about 10 percent lower than the corresponding fine, 10-pitch HCRG at their primary response rotational speeds.

7. The errorless 8-pitch HCRG has a root tooth stress about 6 to 12 percent lower than the corresponding 8-pitch LCRG at their primary response rotational speeds.

These limited results from applying the gear analysis to some sample gears show the need for a systematic parametric analysis of not only HCRG but also LCRG. Such a parametric analysis is necessary to understand fully the effects of the various operating variables and design characteristics, so that optimum spur gear designs can be realized and meaningful gear fatigue tests can be conducted.

## Acknowledgment

## References

1. Frint, H. K.; and Paul, W. F. P.: Design and Evaluation of High Contact Ratio Gearing, Design Phase II. Sikorsky Aircraft Report; July 16, 1974.

2. Richardson, H. H.: Static and Dynamic Load, Stresses and Deflection Cycles in Spur Gear Systems. Dynamic and Control Laboratory Research Memorandum 7454-1, M.I.T., June 30, 1958.

3. Howland, J. S.: An Investigation of Dynamic Loads in Spur-Gear Teeth. Master's thesis, M.I.T. Report, Feb. 1972.

4. Richardson, H. H.: Static and Dynamic Load, Stresses, and Deflection Cycles in Spur-Gear Systems. Sc.D thesis, M.I.T. Report, 1958.

5. Black, J. I.: Summary of Program for the Determination of Dynamic Loads in High Speed Gears. Internal Hamilton Standard Report, May 8, 1961.

6. Metzger, W. W.: Dynamic Loads in the Ryder Gear Test Specimen. Internal Hamilton Standard Report, Sept. 13, 1968.

7. Bollinger, J. G.: An Investigation of New Linear Geared Torsional Systems Using Analog Techniques. Ph. D. thesis, University of Wisconsin, 1961.

8. Ichinoru, K.; and Hirano, F.: Dynamic Behavior of Heavy-Loaded Spur Gears. ASME Preprint 73-PTG-14, 1972.

9. Weber, C.: The Deformations of Loaded Gears and the Effect on Their Load-Carrying Capacity. Sponsored Research (Germany), British Department of Scientific and Industrial Research, Report No. 3 (1949).

10. Heywood, R. B.: Designing by Photoelasticity. Chapman and Hall, Ltd., 1952.